ROYAL SOCIETY OF CHEMISTRY

Check for updates

Understanding the catalytic performances of metal-doped Ta$_2$O$_5$ catalysts for acidic oxygen evolution reaction with computations†

Congcong Han [ab] and Tao Wang [*bcd]

The design of stable and active alternative catalysts to iridium oxide for the anodic oxygen evolution reaction (OER) has been a long pursuit in acidic water splitting. Tantalum pentoxide (Ta$_2$O$_5$) has the merit of great acidic stability but poor OER performance, yet strategies to improve its intrinsic OER activity are highly desirable. Herein, by using density functional theory (DFT) calculations combined with aqueous stability assessment from surface Pourbaix diagrams, we systematically evaluated the OER activity and acidic stability of 14 different metal-doped Ta$_2$O$_5$ catalysts. Apart from the experimentally reported Ir-doped Ta$_2$O$_5$, we computationally identified Ru- and Nb-doped Ta$_2$O$_5$ catalysts as another two candidates with reasonably high stability and activity in acidic OER. Our study also underscores the essence of considering stable surface states of catalysts under working conditions before a reasonable activity trend can be computationally achieved.

1. Introduction

Water splitting for hydrogen (H$_2$) production driven by sustainable energies plays a vital role in the roadmap of carbon neutrality due to the high energy density and zero emission during the utilization of H$_2$.[1–3] Currently, multiple strategies with different devices have been developed for effective water electrolysis, such as alkaline water electrolyzer (AWE),[4] polymer electrolyte membrane water electrolyzer (PEM-WE),[5] solid oxide water electrolyzer (SOWE)[6] and anion exchange membrane water electrolyzer (AEM-WE).[7] Among them, PEM-WE shows advantages of high current densities, high compatibility to intermittent electricity from sustainable energy and a compact cell with a small footprint.[8] Unfortunately, the large-scale application of PEM-WEs is hindered by the heavy reliance on the scarce noble-metals platinum (Pt) and iridium (Ir) as the cathode for the hydrogen evolution reaction (HER) and anode oxygen evolution reaction (OER) catalyst, respectively.[9–12] Indeed, this fundamental obstacle hampering the further development of PEM-WEs triggered

extensive research efforts in developing earth-abundant catalysts as alternatives to Pt and IrO$_x$.

Currently, a group of non-noble metal oxides, particularly 3d transition metal oxides, have been experimentally identified as promising acidic OER catalysts,[13–17] such as CoMnO$_x$,[18] γ-MnO$_2$,[19,20] Ti–MnO$_2$,[21] Co$_3$O$_4$,[22,23] CoFePbO$_x$,[24] Mn$_x$Sb$_{1-x}$O$_z$,[25] and LaMn@Co-ZIF.[26] In principle, the ideal OER catalyst should have high acidic stability, high activity, and low cost, while most candidates only meet two of the three merits. From the viewpoint of practical application, high acidic stability should be the highest priority. Among the reported non-noble metal oxides in the literature, tantalum pentoxide (Ta$_2$O$_5$) is extremely stable in acid but has poor OER activity.[27,28] In principle, Ta$_2$O$_5$ would be an ideal candidate if adequate strategies could be used to improve its OER activity while preserving its high stability, despite having a wide bandgap in the bulk and poor charge transport.[29] Noteworthily, economic viability should be considered before using Ta$_2$O$_5$ as a practical OER catalyst because Ta also has essential applications in resistive switching memories as a high-tech material.[30] Indeed, doping has offered a promising avenue for improving the catalytic activity of materials by altering the d-orbital electronic structure, which governs bond formation or breakage involving oxygen-containing intermediates at active sites.[31–33] Cationic doping and anionic doping have already been extensively explored to enhance the intrinsic OER activity of Ru- and Ir-based oxides.[34–46] Doping with various metal elements, including Ti,[47] Ni,[48,49] Co,[50] La,[26] Fe,[48,51] Zn,[52] Cu,[53] Ce,[54] Mn,[26,55] and Nb,[56,57] has shown the ability to enhance the acidic OER activity and stability of pristine materials. Meanwhile, recent advancements in computations and machine learning have played a crucial role in understanding the fundamental principles governing acid-stable OER catalysts

aDepartment of Chemistry, Zhejiang University, Hangzhou 310058, Zhejiang Province, China

bCenter of Artificial Photosynthesis for Solar Fuels and Department of Chemistry, School of Science and Research Center for Industries of the Future, Westlake University, 600 Dunyu Road, Hangzhou 310030, Zhejiang Province, China. E-mail: twang@westlake.edu.cn

cInstitute of Natural Sciences, Westlake Institute for Advanced Study, 18 Shilongshan Road, Hangzhou 310024, Zhejiang Province, China

dDivision of Solar Energy Conversion and Catalysis at Westlake University, Zhejiang Baima Lake Laboratory Co., Ltd, Hangzhou 310000, Zhejiang, China

† Electronic supplementary information (ESI) available. See DOI: https://doi.org/10.1039/d4sc03554b

and also facilitated the rational design of materials with improved performance and durability.[58–66]

In this work, we focus on levering computational approaches combined with the doping strategy to understand the acidic OER mechanism and activity of metal-doped Ta_2O_5 (M = Ti, V, Cr, Mn, Fe, Co, Ni, Zr, Nb, Mo, Sn, Sb, Ru, and Ir). Our systematic density functional theory (DFT) calculations of the adsorbate evolution mechanism (AEM) on the 14 M-doped Ta_2O_5 catalysts, as well as aqueous stability evaluation, clearly revealed their stability and activity trend in acidic OER, where the Ir-, Ru-, and Nb-doped Ta_2O_5 systems were theoretically predicted to be promising candidates with good performances. Our stability analysis with surface Pourbaix diagrams indicates the essence of considering the stable surface state of catalysts under working conditions when conducting computational screening of electrocatalysts.

2. Methods and models

All calculations were carried out by spin-polarized density functional theory (DFT) as implemented in the Vienna *Ab initio* Simulation Package (VASP) interfaced with the atomistic simulation environment (ASE) within the projector augmented wave method (PAW).[67,68] The generalized gradient approximation (GGA) in the scheme of revised-Perdew–Burke–Ernzerhof (RPBE) was employed to describe the exchange and correlation interaction.[69,70] A plane-wave basis set with a kinetic energy cut-off of 500 eV is used for all calculations. The convergence criteria for electronic energy and forces during structural optimization are 1.0×10^{-5} eV and 0.02 eV Å^{-1}, while those for frequency calculation are 1.0×10^{-7} eV and 0.02 eV Å^{-1}, respectively.

Ta_2O_5 has several crystalline structures, while the λ phase with the *Pbam* space group was chosen for further calculation in this work. The optimized bulk structure had lattice parameters of $a = 6.29$ Å, $b = 7.47$ Å, and $c = 3.84$ Å, which agreed well with experimental values ($a = 6.22$ Å, $b = 7.36$ Å, and $c = 3.90$ Å).[71–74] The (100) surface was chosen as the model for OER mechanism simulation due to its high stability and wide experimental characterization, while both Ta ($Ta_{16}O_{40}$) and O ($Ta_{16}O_{42}$) terminations were considered. The p (1 × 2) slab contained four metal layers, while the top two layers were relaxed and the bottom two
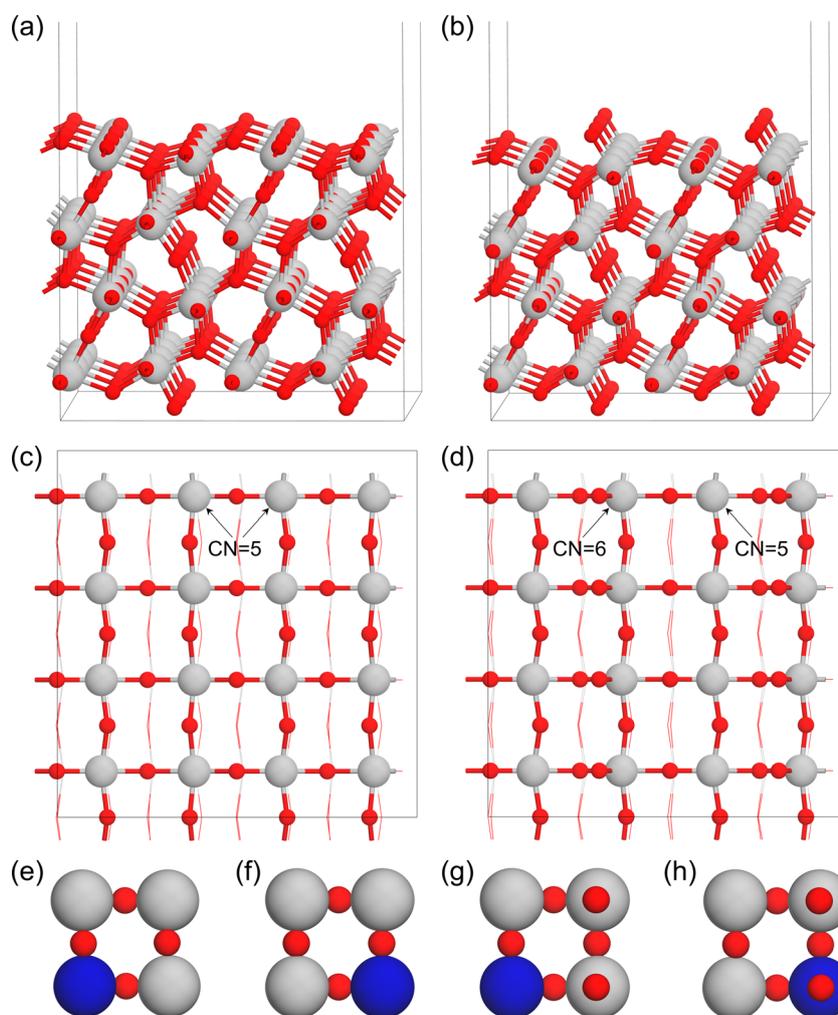

Fig. 1 The side (a and b) and top (c and d) views of Ta- and O-terminations of Ta_2O_5, as well as the metal-doped Ta-termination (e and f) and O-termination (g and h) of Ta_2O_5. (The red, grey, and bright blue spheres represent O, Ta, and dopant atoms, respectively).

layers were fixed. A vacuum layer of 15 Å is applied in the z-direction of the slab to avoid interactions. A $3 \times 3 \times 1$ gamma centered k-point meshes was used to sample the Brillouin zone. The vibrational frequencies of adsorbates on the surfaces were analyzed, while free energies were calculated within the harmonic approximation. The OER mechanism was simulated within the framework of the computational hydrogen electrode (CHE),[75] which is detailed in the ESI.† The stability of the metal-doped Ta_2O_5 was evaluated by using formation energy (E_f) and cohesive energy (E_{coh}), where a more negative value of E_f indicates higher synthetic feasibility and a more positive value of E_{coh} indicates higher thermodynamic stability.[48,76] More details for calculating E_f and E_{coh} are summarized in the ESI.†

3. Results and discussion

3.1 Structure and stability of metal-doped Ta_2O_5 (100) surfaces

To evaluate the roles of transition metals in tuning the properties of the Ta_2O_5 catalyst for the high-performance OER, we applied the substitutional approach by replacing the surface Ta with different metals (M = Ti, V, Cr, Mn, Fe, Co, Ni, Zr, Nb, Mo, Sn, Sb, Ru, and Ir). As shown in Fig. 1a–d, the λ-Ta_2O_5 (100)

Fig. 2 (a) Formation energy (E_f) and (b) cohesive energy (E_{coh}) of M–$Ta_{15}O_{40}$ and M–$Ta_{15}O_{42}$.

surface has both Ta ($Ta_{16}O_{40}$) and O ($Ta_{16}O_{42}$) terminations. For the Ta-termination shown in Fig. 1c, there are two types of surface Ta atoms with five coordination environments. Therefore, we considered two substitutional models in Fig. 1e and f (M–$Ta_{15}O_{40}$). For the O-termination shown in Fig. 1b and d, there are also two types of Ta atoms with different coordination environments on the surface shown in Fig. 1d (M–$Ta_{15}O_{42}$). Based on the doping sites shown in Fig. 1e–h, we systematically evaluated the stabilities of various metals on these sites, where the most stable doping structures of each metal on both Ta- and O-terminations are summarized in Table S2.†

In principle, the thermodynamic stability of the catalyst will determine whether it could be easily synthesized experimentally. Therefore, we calculated the formation energy (E_f) and cohesive energy (E_{coh}) of all the doped systems. As shown in Fig. 2, the early transition metals (Zr, Ti, Nb, V, and Cr) doped systems generally have very negative values of E_f (Table S2†), indicating their high stabilities. Systems doped by the magnetic Fe, Co, and Ni metals, as well as the noble metal Ir and Ru metals, showed positive values of E_f, which indicates their relatively lower stabilities than the early transition metal doped Ta_2O_5. Considering that the Ir-doped Ta_2O_5 has been successfully synthesized and found to be stable and active for the OER experimentally,[77] we anticipate that catalysts with lower E_f than Ir-doped Ta_2O_5 will show reasonable feasibility to be synthesized experimentally. In this respect, most of these 28 M-doped structures have reasonable synthetic feasibility, at least from a thermodynamic perspective. Meanwhile, the E_{coh} values for all 28 M-doped structures shown in Fig. 2b and Table S2† are higher than 0.5 eV, suggesting their potential high stability upon synthesis.

3.2 OER activity on the metal-doped Ta- and O-terminations of Ta_2O_5 (100)

To have a direct comparison of the OER activity among different catalysts, we systematically simulated the classical adsorbate evolution mechanism (AEM)[78] on these M-doped Ta_2O_5 systems within the framework of computational hydrogen electrode (CHE) as developed by the Nørskov group[79] (more details in the ESI†). As shown in Fig. 3a, the catalytic cycle starts with the deprotonation of H_2O on the active site to form *OH species, followed by another deprotonation step to form the surface *O intermediate. Then, the O–O bond formation takes place via the reaction of *O with another H_2O molecule to form the *OOH intermediate, accompanied by a deprotonation step. Finally, O_2 is formed through the deprotonation of *OOH with the regeneration of the active site.

Based on this mechanism, the reaction free energy change (ΔG) for each step was calculated at 0 V, pH = 0, and $T = 298.15$ K within the framework of the CHE model. Then, the potential-determining step (PDS) is typically the last step to go downhill in free energy as the potential increases. In other words, PDS is the step with the largest ΔG (ΔG_{PDS}) among the four-step OER mechanism in Fig. 3a. The theoretical overpotential (η) can be expressed as (ΔG_{PDS})/$e - 1.23$ V. Using the pristine and Ir-doped Ta_2O_5 as examples, we plotted the potential free energy

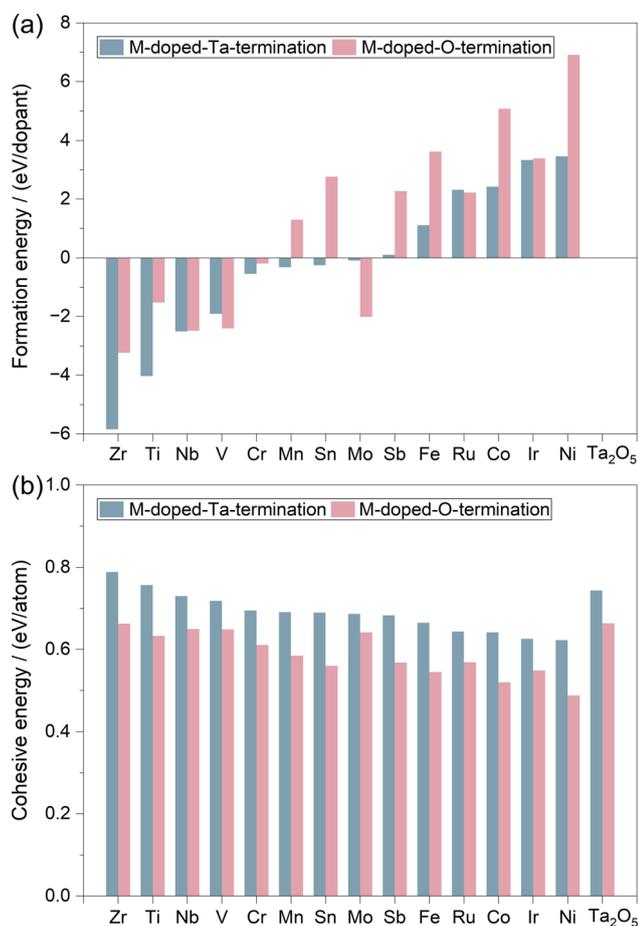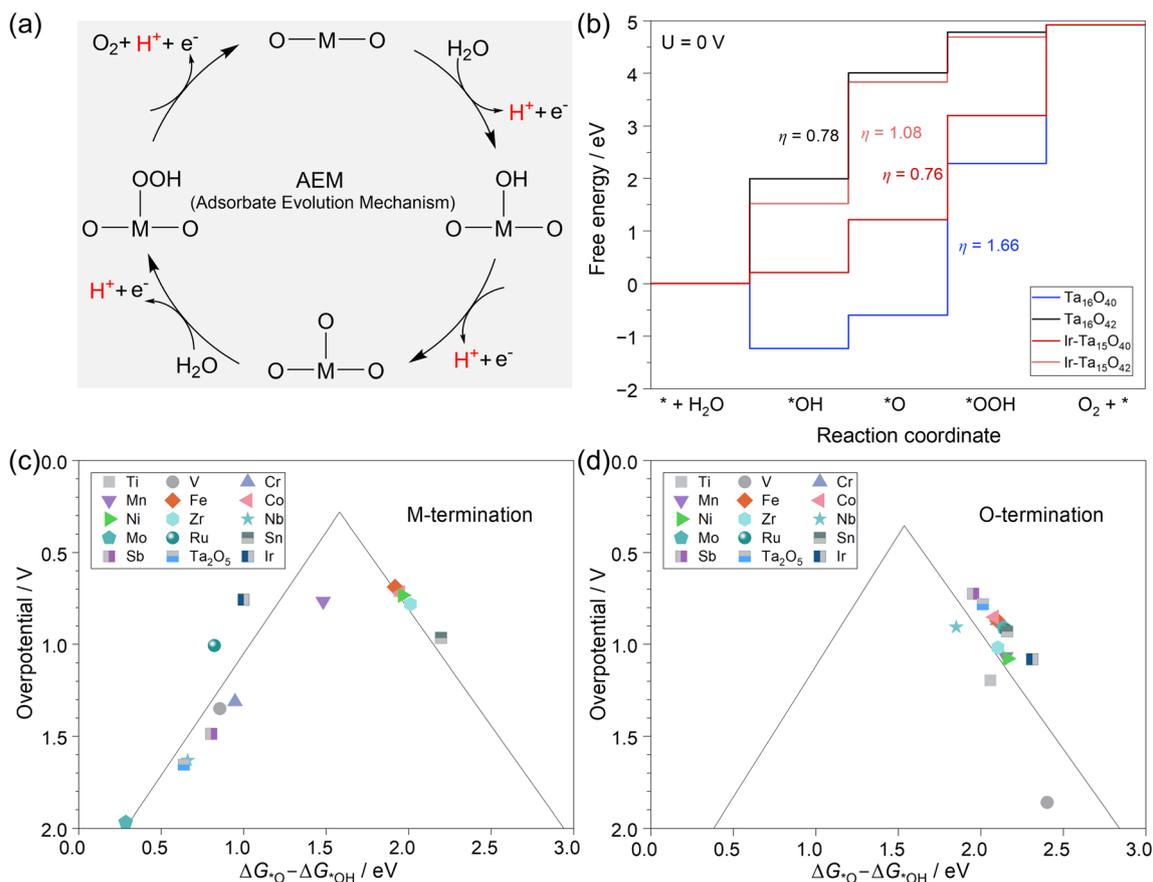**Fig. 3** (a) Classical adsorbate evolution mechanism (AEM) for the oxygen evolution reaction; (b) free energy diagrams of the OER on the two pristine and Ir-doped terminations of the Ta_2O_5 (100) surface; theoretically predicted activity trends toward the OER on metal-doped (c) Ta termination ($M-Ta_{15}O_{40}$) and (d) O termination ($M-Ta_{15}O_{42}$) of the Ta_2O_5 (100) surface.

diagrams of the OER in Fig. 3b. It shows that each system has a different PDS and η, *i.e.*, the PDS in the case of Ta terminations of $Ta_{16}O_{40}$ and Ir-doped Ta_2O_5 is $*O \rightarrow *OOH$ with the η values of 1.66 V and 0.76 V, while that in the case of the O-termination of $Ta_{16}O_{42}$ and Ir-doped Ta_2O_5 becomes $*OH \rightarrow *O$ with the η values of 0.78 V and 1.08 V, respectively.

As per the Sabatier principle, an ideal catalyst requires the binding strength of the key intermediate to be neither too strong nor too weak. Based on the framework established by the Nørskov group,[27] there is a volcano-shaped relationship between η_{OER} and the value of $\Delta G_{*O} - \Delta G_{*OH}$ among a group of materials. Our analysis in Fig. 3c and d also shows the volcanic OER activity trend among 28 $M-Ta_2O_5$ systems, but the two terminations have quite different trends. On the Ta termination in Fig. 3c and Table S3,† most of the cases are located at the left leg of the volcano due to the lower deprotonation energy of surface hydroxide, where the formation of $*OOH$ species is the PDS. At the right leg of the volcano, the weak binding strength of $*O$ makes the deprotonation of $*OH$ species the PDS. Among these doped systems in the case of Ta termination, Fe-doping has the lowest η of 0.69 V, followed by Ti (0.71 V), Co (0.72 V), Ni (0.73 V), Ir (0.76 V), Mn (0.77 V), Sn (0.97 V), and Zr (0.78 V), while the rest of them are higher than 1.0 V.

In the case of the O-termination shown in Fig. 3d and Table S4,† all the metal-doped systems are located at the right leg of the volcano due to the weak binding strength with oxygen, while the deprotonation of $*OH$ species is the PDS. Meanwhile, the activity trend of these 14 doping metals is quite different from that of the Ta termination. Among them, the Sb-doped O-termination has the lowest η of 0.72 V, followed by the pristine $Ta_{15}O_{42}$ (0.78 V).

3.3 Surface structures and OER activity of $M-Ta_2O_5$ under working conditions

The above mechanism studies on the two terminations have clearly revealed that the OER activity is tightly related to the surface structure of $M-Ta_2O_5$. Then, the question becomes, what is the real surface structure of the catalyst under working conditions? To clarify this, we further applied the surface Pourbaix diagram to describe the surface states of each $M-Ta_2O_5$ system at different pH and working potentials.

More specifically, the surface of $M-Ta_2O_5$ will inevitably be covered by different species during the OER, such as $*O$ and $*OH$. We systematically calculated the binding of different species on the surface of pristine and 14 M-doped models to identify the most stable surface composition of each model at
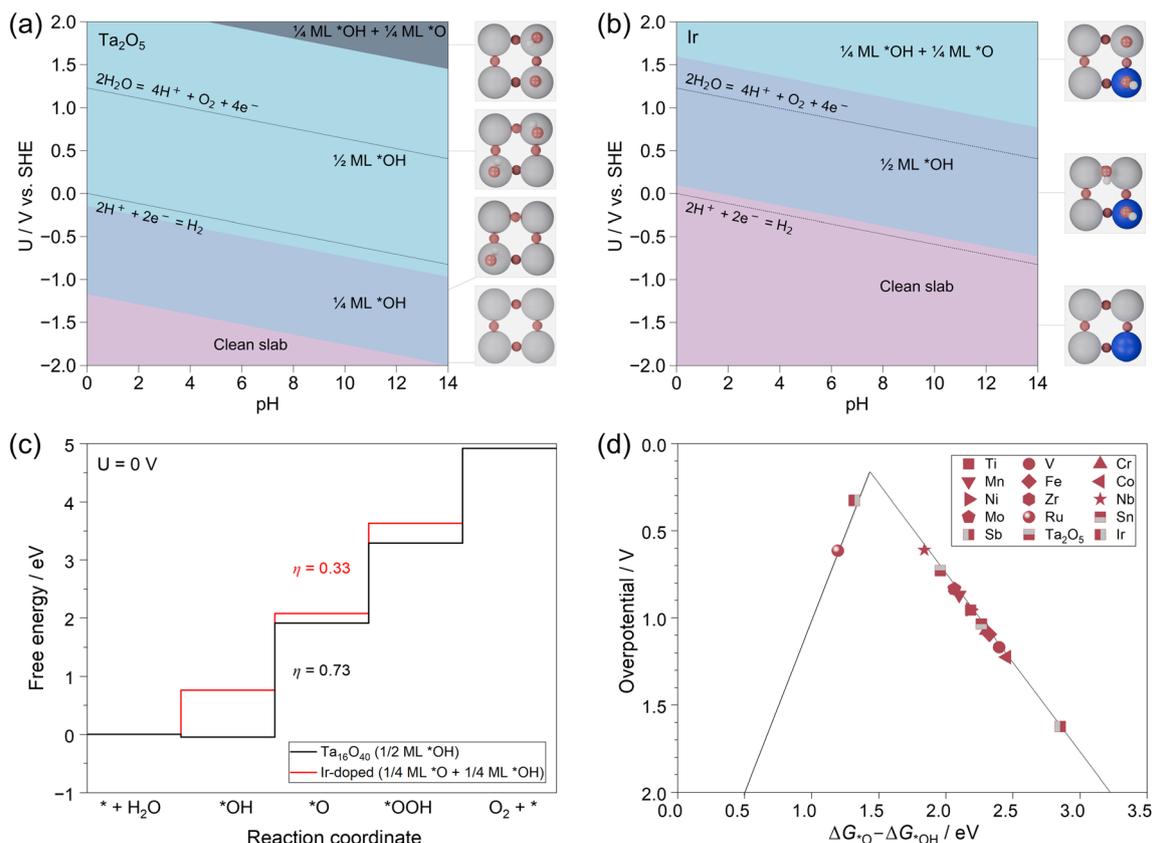
Fig. 4 Surface Pourbaix diagrams of pristine (a) and Ir-doped (b) Ta$_2$O$_5$ (100) surface; free energy diagrams of the OER on the most stable surface states of pristine and Ir-doped Ta$_2$O$_5$ (100) surface at pH = 0 and U = 0 V (c); OER activity trend of M-doped Ta$_2$O$_5$ (100) at the most stable surface states determined by surface Pourbaix diagram analysis (d).

a wide range of pH and potentials. More computational details are shown in the ESI.† We use the electrochemical potential window (EPW) to describe the potential range in which a catalyst can maintain its pristine state at pH = 0.[80] As shown in Fig. 4a, the pristine Ta$_2$O$_5$ (100) surface shows an EPW less than −1.1 V vs. SHE, while it will be covered by 1/4 monolayer (ML) *OH at −1.1 V to −0.1 V as well as 1/2 ML *OH at −0.1–2.0 V. For comparison, Ir-doped Ta$_2$O$_5$ (100) in Fig. 4b exhibits an EPW of less than 0.1 V, while it will be covered by 1/2 ML *OH at 0.1–1.6 V as well as 1/4 ML *OH + 1/4 ML *O at >1.6 V vs. SHE. Similar surface Pourbaix diagrams of the other M-doped systems are summarized in the ESI.† Clearly, it is crucial to consider the specific surface state of the catalyst under electrochemical operating conditions. In this respect, the OER mechanism investigation was conducted on the most stable surface state of each M-doped Ta$_2$O$_5$, where a potential of ~1.60 V was chosen based on experimental setups.[81] The calculated free energies of intermediates and the derived overpotentials are listed in Table S6.†

As shown in Fig. 4c, the 1/2 ML *OH covered Ta-termination is the most stable state of the Ta$_2$O$_5$ (100) surface at pH = 0 and 1.6 V vs. SHE, where the theoretical overpotential is calculated to be 0.73 V with *OH → *O being the PDS. For the Ir-doped system, the surface is covered by 1/4 ML *O and 1/4 ML *OH

at pH = 0 and 1.6 V vs. SHE, where the calculated η is only 0.33 V.

Finally, we have summarized the theoretical overpotentials calculated from the most stable surface states of each M-doped Ta$_2$O$_5$ in Fig. 4d for comparison. It shows that most of the systems are located at the right leg of the volcano except the Ir-doped and Ru-doped Ta$_2$O$_5$. Among them, the Ir-doped Ta$_2$O$_5$ is closest to the peak of the volcano, which has the η of only 0.33 V and an optimum $\Delta G_{*O} - \Delta G_{*OH}$ of ~1.32 eV. Meanwhile, the Ru-doped and Nb-doped Ta$_2$O$_5$ also exhibit relatively low theoretical overpotentials of 0.62 V and 0.61 V. Noteworthily, the calculated η values of these catalysts are different from those of pure Ta- and O-terminations shown in Fig. 3, again indicating the essence of considering the stable surface state of catalysts under working conditions.

4. Conclusion

In summary, we conducted density functional theory calculations to systematically investigate the thermodynamic stability, aqueous stability, and acidic OER activity of various metal-doped (metal = Ti, V, Cr, Mn, Fe, Co, Ni, Zr, Nb, Mo, Sn, Sb, Ru, Ir) Ta$_2$O$_5$ (100) surfaces. Our calculated formation energies and cohesive energies of these 14 systems showed their reasonably high stability thermodynamically, thereby, a high

experimental synthetic feasibility. Then, the most stable surface state of each M-doped Ta_2O_5 (100) surface at different pH and potential ranges was evaluated by using the surface Pourbaix diagrams. Further OER activity evaluations of these catalysts were based on the adsorbate evolution mechanism (AEM), where the Ir-doped Ta_2O_5 with the lowest theoretical overpotential of 0.33 V was computationally predicted to be most promising and consistent with experimental findings in the literature. Meanwhile, Ru- and Nb-doped catalysts were also predicted to be stable and active for acidic OER with theoretical overpotentials of 0.62 V and 0.61 V, respectively. Additionally, we note that electrochemical-driven pre-adsorption of species on the catalysts dramatically influence the OER activity. Therefore, it is crucial to analyze the surface state of a catalyst under electrochemical conditions with the surface Pourbaix diagram before conducting a detailed mechanism simulation. Our results not only adequately illustrated the general OER activity trend of metal-doped Ta_2O_5 catalysts but also provided theoretical guidance for further experimental studies of these systems.

Data availability

Computational details and other results supporting the main conclusions are summarized in the ESI.† Other data supporting this article have been included as part of the ESI (dataset.txt).†

Author contributions

T. W. conceived and supervised this project; C. C. H. performed all the DFT computations, data analysis, and figure drawing; all authors discussed the results and contributed to the writing of the manuscript.

Conflicts of interest

The authors declare no competing financial interest.

Acknowledgements

References

1 S. Sharma and S. K. Ghoshal, *Renewable Sustainable Energy Rev.*, 2015, **43**, 1151–1158.

2 G. Nicoletti, N. Arcuri, G. Nicoletti and R. Bruno, *Energy Convers. Manage.*, 2015, **89**, 205–213.

3 K. Ayers, N. Danilovic, R. Ouimet, M. Carmo, B. Pivovar and M. Bornstein, *Annu. Rev. Chem. Biomol. Eng.*, 2019, **10**, 219–239.

4 M. David, C. Ocampo-Martínez and R. Sánchez-Peña, *J. Energy Storage*, 2019, **23**, 392–403.

5 M. Carmo, D. L. Fritz, J. Mergel and D. Stolten, *Int. J. Hydrogen Energy*, 2013, **38**, 4901.

6 Y. Xu, S. Cai, B. Chi and Z. Tu, *Int. J. Hydrogen Energy*, 2024, **50**, 548–591.

7 I. Vincent and D. Bessarabov, *Renewable Sustainable Energy Rev.*, 2018, **81**, 1690–1704.

8 S. A. Grigoriev, V. I. Porembsky and V. N. Fateev, *Int. J. Hydrogen Energy*, 2006, **31**, 171–175.

9 O. Diaz-Morales, S. Raaijman, R. Kortlever, P. J. Kooyman, T. Wezendonk, J. Gascon, W. T. Fu and M. T. M. Koper, *Nat. Commun.*, 2016, **7**, 12363.

10 L. Zhang, K. Doyle-Davis and X. Sun, *Energy Environ. Sci.*, 2019, **12**, 492–517.

11 F. Liao, K. Yin, Y. Ji, W. Zhu, Z. Fan, Y. Li, J. Zhong, M. Shao, Z. Kang and Q. Shao, *Nat. Commun.*, 2023, **14**, 1248.

12 J. Xu, H. Jin, T. Lu, J. Li, Y. Liu, K. Davey, Y. Zheng and S. Qiao, *Sci. Adv.*, 2023, **9**, eadh1718.

13 R. Subbaraman, D. Tripkovic, K. Chang, D. Strmcnik, A. P. Paulikas, P. Hirunsit, M. Chan, J. Greeley, V. Stamenkovic and N. M. Markovic, *Nat. Mater.*, 2012, **11**, 550–557.

14 M. Huynh, D. K. Bediako and D. G. Nocera, *J. Am. Chem. Soc.*, 2014, **136**, 6002–6010.

15 W. Xiong, H. Yin, T. Wu and H. Li, *Chem.–Eur. J.*, 2023, **29**, e202202872.

16 N. Wang, P. Ou, R. K. Miao, Y. Chang, Z. Wang, S. Hung, J. Abed, A. Ozden, H. Chen, H. Wu, J. E. Huang, D. Zhou, W. Ni, L. Fan, Y. Yan, T. Peng, D. Sinton, Y. Liu, H. Liang and E. H. Sargent, *J. Am. Chem. Soc.*, 2023, **145**, 7829–7836.

17 X. Zhang, C. Feng, B. Dong, C. Liu and Y. Chai, *Adv. Mater.*, 2023, **35**, 2207066.

18 A. Li, S. Kong, C. Guo, H. Ooka, K. Adachi, D. Hashizume, Q. Jiang, H. Han, J. Xiao and R. Nakamura, *Nat. Catal.*, 2022, **5**, 109–118.

19 A. Li, H. Ooka, N. Bonnet, T. Hayashi, Y. Sun, Q. Jiang, C. Li, H. Han and R. Nakamura, *Angew. Chem., Int. Ed.*, 2019, **58**, 5054–5058.

20 S. Kong, A. Li, J. Long, K. Adachi, D. Hashizume, Q. Jiang, K. Fushimi, H. Ooka, J. Xiao and R. Nakamura, *Nat. Catal.*, 2024, **7**, 252–261.

21 R. Frydendal, E. A. Paoli, I. Chorkendorff, J. Rossmeisl and I. E. L. Stephens, *Adv. Energy Mater.*, 2015, **5**, 1500991.

22 J. Huang, H. Sheng, R. D. Ross, J. Han, X. Wang, B. Song and S. Jin, *Nat. Commun.*, 2021, **12**, 3036.

23 J. Yu, F. A. Garcés-Pineda, J. González-Cobos, M. Peña-Díaz, C. Rogero, S. Giménez, M. C. Spadaro, J. Arbiol, S. Barja and J. R. Galán-Mascarós, *Nat. Commun.*, 2022, **13**, 4341.

24 M. Chatti, J. L. Gardiner, M. Fournier, B. Johannessen, T. Williams, T. R. Gengenbach, N. Pai, C. Nguyen, D. R. MacFarlane, R. K. Hocking and A. N. Simonov, *Nat. Catal.*, 2019, **2**, 457–465.

25 L. Zhou, A. Shinde, J. H. Montoya, A. Singh, S. Gul, J. Yano, Y. Ye, E. J. Crumlin, M. H. Richter, J. K. Cooper, H. S. Stein, J. A. Haber, K. A. Persson and J. M. Gregoire, *ACS Catal.*, 2018, **8**, 10938–10948.

26 L. Chong, G. Gao, J. Wen, H. Li, H. Xu, Z. Green, J. D. Sugar, A. J. Kropf, W. Xu, X. Lin, H. Xu, L. Wang and D.-J. Liu, *Science*, 2023, **380**, 609–616.

27 I. C. Man, H. Su, F. Calle-Vallejo, H. A. Hansen, J. I. Martínez, N. G. Inoglu, J. Kitchin, T. F. Jaramillo, J. K. Nørskov and J. Rossmeisl, *ChemCatChem*, 2011, **3**, 1159–1165.

28 Z. Wang, X. Guo, J. Montoya and J. K. Nørskov, *npj Comput. Mater.*, 2020, **6**, 160.

29 H. Chen, G. Feng, W. Fan, J. Han, Y. Li and Q. Lai, *Opt. Mater. Express*, 2019, **9**, 3132–3145.

30 M. Lee, C. B. Lee, D. Lee, S. R. Lee, M. Chang, J. H. Hur, Y. Kim, C. Kim, D. H. Seo, S. Seo, U. I. Chung, I. Yoo and K. Kim, *Nat. Mater.*, 2011, **10**, 625–630.

31 S. Sun, X. Zhou, B. Cong, W. Hong and G. Chen, *ACS Catal.*, 2020, **10**, 9086–9097.

32 S. R. Ede and Z. Luo, *J. Mater. Chem. A*, 2021, **9**, 20131–20163.

33 X. Zheng, Y. Chen, W. Lai, P. Li, C. Ye, N. Liu, S. X. Dou, H. Pan and W. Sun, *Adv. Funct. Mater.*, 2022, **32**, 2200663.

34 M. Retuerto, L. Pascual, F. Calle-Vallejo, P. Ferrer, D. Gianolio, A. G. Pereira, Á. García, J. Torrero, M. T. Fernández-Díaz, P. Bencok, M. A. Peña, J. L. G. Fierro and S. Rojas, *Nat. Commun.*, 2019, **10**, 2041.

35 S. Hao, M. Liu, J. Pan, X. Liu, X. Tan, N. Xu, Y. He, L. Lei and X. Zhang, *Nat. Commun.*, 2020, **11**, 5368.

36 R. R. Rao, M. J. Kolb, L. Giordano, A. F. Pedersen, Y. Katayama, J. Hwang, A. Mehta, H. You, J. R. Lunger, H. Zhou, N. B. Halck, T. Vegge, I. Chorkendorff, I. E. L. Stephens and Y. Shao-Horn, *Nat. Catal.*, 2020, **3**, 516–525.

37 Y. Wen, P. Chen, L. Wang, S. Li, Z. Wang, J. Abed, X. Mao, Y. Min, C. T. Dinh, P. D. Luna, R. Huang, L. Zhang, L. Wang, L. Wang, R. J. Nielsen, H. Li, T. Zhuang, C. Ke, O. Voznyy, Y. Hu, Y. Li, W. A. Goddard III, B. Zhang, H. Peng and E. H. Sargent, *J. Am. Chem. Soc.*, 2021, **143**, 6482–6490.

38 L. Zhou, Y. Shao, F. Yin, J. Li, F. Kang and R. Lv, *Nat. Commun.*, 2023, **14**, 7644.

39 Y. Xue, J. Zhao, L. Huang, Y. Lu, A. Malek, G. Gao, Z. Zhuang, D. Wang, C. T. Yavuz and X. Lu, *Nat. Commun.*, 2023, **14**, 8093.

40 Z. Shi, J. Li, Y. Wang, S. Liu, J. Zhu, J. Yang, X. Wang, J. Ni, Z. Jiang, L. Zhang, Y. Wang, C. Liu, W. Xing and J. Ge, *Nat. Commun.*, 2023, **14**, 843.

41 X. Wang, H. Jang, S. Liu, Z. Li, X. Zhao, Y. Chen, M. G. Kim, Q. Qin and X. Liu, *Adv. Energy Mater.*, 2023, **13**, 2301673.

42 D. Galyamin, J. Torrero, I. Rodríguez, M. J. Kolb, P. Ferrer, L. Pascual, M. A. Salam, D. Gianolio, V. Celorrio, M. Mokhtar, D. G. Sanchez, A. S. Gago, K. A. Friedrich, M. A. Peña, J. A. Alonso, F. Calle-Vallejo, M. Retuerto and S. Rojas, *Nat. Commun.*, 2023, **14**, 2010.

43 S. Chen, S. Zhang, L. Guo, L. Pan, C. Shi, X. Zhang, Z. Huang, G. Yang and J.-J. Zou, *Nat. Commun.*, 2023, **14**, 4127.

44 X. Zheng, J. Yang, P. Li, Q. Wang, J. Wu, E. Zhang, S. Chen, Z. Zhuang, W. Lai, S. Dou, W. Sun, D. Wang and Y. Li, *Sci. Adv.*, 2023, **9**, eadi8025.

45 Y. Wang, X. Lei, B. Zhang, B. Bai, P. Das, T. Azam, J. Xiao and Z.-S. Wu, *Angew. Chem., Int. Ed.*, 2024, **63**, e202316903.

46 X. Ping, Y. Liu, L. Zheng, Y. Song, L. Guo, S. Chen and Z. Wei, *Nat. Commun.*, 2024, **15**, 2501.

47 H. Li, Y. Xu, N. Lv, Q. Zhang, X. Zhang, Z. Wei, Y. Wang, H. Tang and H. Pan, *ACS Sustainable Chem. Eng.*, 2023, **11**, 1121–1132.

48 Y. Peng, H. Hajiyani and R. Pentcheva, *ACS Catal.*, 2021, **11**, 5601–5613.

49 Z. Wu, F. Chen, B. Li, S. Yu, Y. Z. Finfrock, D. M. Meira, Q. Yan, P. Zhu, M. Chen, T. Song, Z. Yin, H. Liang, S. Zhang, G. Wang and H. Wang, *Nat. Mater.*, 2023, **22**, 100–108.

50 Y. Tian, S. Wang, E. Velasco, Y. Yang, L. Cao, L. Zhang, X. Li, Y. Lin, Q. Zhang and L. Chen, *iScience*, 2020, **23**, 100756.

51 P. Ye, K. Fang, H. Wang, Y. Wang, H. Huang, C. Mo, J. Ning and Y. Hu, *Nat. Commun.*, 2024, **15**, 1012.

52 D. Zhang, M. Li, X. Yong, H. Song, G. I. N. Waterhouse, Y. Yi, B. Xue, D. Zhang, B. Liu and S. Lu, *Nat. Commun.*, 2023, **14**, 2517.

53 Y. Feng, S. Si, G. Deng, Z. Xu, Z. Pu, H. Hu and C. Wang, *J. Alloys Compd.*, 2022, **892**, 162113.

54 T. Audichon, S. Morisset, T. W. Napporn, K. B. Kokoh, C. Comminges and C. Morais, *ChemElectroChem*, 2015, **2**, 1128–1137.

55 S. Chen, H. Huang, P. Jiang, K. Yang, J. Diao, S. Gong, S. Liu, M. Huang, H. Wang and Q. Chen, *ACS Catal.*, 2020, **10**, 1152–1160.

56 N. Todoroki, R. Kudo, K. Hayashi, M. Yokoi, N. Naraki and T. Wadayama, *ACS Catal.*, 2023, **13**, 11433–11440.

57 W. Hu, S. Chen and Q. Xia, *Int. J. Hydrogen Energy*, 2014, **39**, 6967–6976.

58 G. T. K. K. Gunasooriya and J. K. Nørskov, *ACS Energy Lett.*, 2020, **5**, 3778–3787.

59 J. Peng, L. Giordano, T. C. Davenport and Y. Shaohorn, *Chem. Mater.*, 2022, **34**, 7774–7787.

60 S. Jo, M.-C. Kim, K. B. Lee, H. Choi, L. Zhang and J. I. Sohn, *Adv. Energy Mater.*, 2023, **13**, 2301420.

61 A. Badreldin, O. Bouhali and A. Abdel-Wahab, *Adv. Funct. Mater.*, 2023, **34**, 2312425.

62 X. Mao, L. Wang and Y. Li, *J. Phys. Chem. Lett.*, 2023, **14**, 170–177.

63 J. Moon, W. Beker, M. Siek, J. Kim, H. S. Lee, T. Hyeon and B. A. Grzybowski, *Nat. Mater.*, 2024, **23**, 108–115.

64 H. Park, Y. Kim, S. Choi and H. J. Kim, *J. Energy Chem.*, 2024, **91**, 645–655.

65 Z. Fang, S. Li, Y. Zhang, Y. Wang, K. Meng, C. Huang and S. Sun, *J. Phys. Chem. Lett.*, 2024, **15**, 281–289.

66 J. A. Esterhuizen, A. Mathur, B. R. Goldsmith and S. Linic, *J. Am. Chem. Soc.*, 2024, **146**, 5511–5522.

67 P. E. Blöchl, *Phys. Rev. B: Condens. Matter Mater. Phys.*, 1994, **50**, 17953–17979.

68 A. H. Larsen, J. J. Mortensen, J. Blomqvist, I. E. Castelli, R. Christensen, M. Dułak, J. Friis, M. N. Groves,

B. Hammer, C. Hargus, E. D. Hermes, P. C. Jennings, P. B. Jensen, J. Kermode, J. R. Kitchin, E. L. Kolsbjerg, J. Kubal, K. Kaasbjerg, S. Lysgaard, J. B. Maronsson, T. Maxson, T. Olsen, L. Pastewka, A. Peterson, C. Rostgaard, J. Schiøtz, O. Schütt, M. Strange, K. S. Thygesen, T. Vegge, L. Vilhelmsen, M. Walter, Z. Zeng and K. W. Jacobsen, *J. Phys.: Condens. Matter*, 2017, **29**, 273002.

69 J. P. Perdew, K. Burke and M. Ernzerhof, *Phys. Rev. Lett.*, 1996, **77**, 3865–3868.

70 B. Hammer, L. B. Hansen and J. K. Nørskov, *Phys. Rev. B: Condens. Matter Mater. Phys.*, 1999, **59**, 7413–7421.

71 L. A. Aleshina and S. V. Loginova, *Crystallogr. Rep.*, 2002, **47**, 415–419.

72 S. H. Lee, J. S. Kim, J. S. Kim, S. J. Kim and G. S. Park, *Phys. Rev. Lett.*, 2013, **110**, 1–5.

73 Y. Yang and Y. Kawazoe, *Phys. Rev. Mater.*, 2018, **2**, 034602.

74 C. Han and T. Wang, *Energy Fuels*, 2023, **37**, 13624–13644.

75 T. Murase, H. Irie and K. Hashimoto, *J. Phys. Chem. B*, 2004, **108**, 15803–15807.

76 S. Cao, H. Chen, Y. Hu, J. Li, C. Yang, Z. Chen, S. Wei, S. Liu, Z. Wang, D. Sun and X. Lu, *Chem. Eng. J.*, 2023, **461**, 141936.

77 Y. Zheng, J. Vernieres, Z. Wang, K. Zhang, D. Hochfilzer, K. Krempl, T. Liao, F. Presel, T. Altantzis, J. Fatermans, S. B. Scott, N. M. Secher, C. Moon, P. Liu, S. Bals, S. Van Aert, A. Cao, M. Anand, J. K. Nørskov, J. Kibsgaard and I. Chorkendorff, *Nat. Energy*, 2022, **7**, 55–64.

78 C. Rong, K. Dastafkan, Y. Wang and C. Zhao, *Adv. Mater.*, 2023, **35**, 2211884.

79 J. K. Nørskov, J. Rossmeisl, A. Logadottir, L. Lindqvist, J. R. Kitchin, T. Bligaard and H. Jónsson, *J. Phys. Chem. B*, 2004, **108**, 17886–17892.

80 W. Yang, Z. Jia, B. Zhou, L. Wei, Z. Gao and H. Li, *Commun. Chem.*, 2023, **6**, 6.

81 X. Han, X. Ling, D. Yu, D. Xie, L. Li, S. Peng, C. Zhong, N. Zhao, Y. Deng and W. Hu, *Adv. Mater.*, 2019, **31**, 1905622.